

MDM2 antagonists promote CRISPR/Cas9-mediated precise genome editing in sheep primary cells

Yan Li,^{1,2,3,6} Di Lian,^{2,6} Jiahao Wang,^{1,4,6} Yue Zhao,¹ Yao Li,¹ Guoshi Liu,¹ Sen Wu,² Shoulong Deng,⁵ Xuguang Du,² and Zhengxing Lian¹

¹Beijing Key Laboratory for Animal Genetic Improvement, National Engineering Laboratory for Animal Breeding, College of Animal Science and Technology, China Agricultural University, Beijing 100193, China; ²State Key Laboratory of Agrobiotechnology, College of Biological Sciences, China Agricultural University, Beijing 100193, China; ³Laboratory Animal Center of the Academy of Military Medical Sciences, Beijing 100071, China; ⁴Department of Biomedical Engineering, College of Future Technology, Peking University, Beijing 100871, China; ⁵NHC Key Laboratory of Human Disease Comparative Medicine, Institute of Laboratory Animal Sciences, Chinese Academy of Medical Sciences and Comparative Medicine Center, Peking Union Medical College, Beijing 100021, China; ⁶These authors contributed equally

CRISPR-Cas9-mediated genome editing in sheep is of great use in both agricultural and biomedical applications. While targeted gene knockout by CRISPR-Cas9 through non-homologous end joining (NHEJ) has worked efficiently, the knockin efficiency via homology-directed repair (HDR) remains lower, which severely hampers the application of precise genome editing in sheep. Here, in sheep fetal fibroblasts (SFFs), we optimized several key parameters that affect HDR, including homology arm (HA) length and the amount of double-stranded DNA (dsDNA) repair template; we also observed synchronization of SFFs in G2/M phase could increase HDR efficiency. Besides, we identified three potent small molecules, RITA, Nutlin3, and CTX1, inhibitors of p53-MDM2 interaction, that caused activation of the p53 pathway, resulting in distinct G2/M cell-cycle arrest in response to DNA damage and improved CRISPR-Cas9-mediated HDR efficiency by 1.43- to 4.28-fold in SFFs. Furthermore, we demonstrated that genetic knockout of *p53* could inhibit HDR in SFFs by suppressing the expression of several key factors involved in the HDR pathway, such as *BRCA1* and *RAD51*. Overall, this study offers an optimized strategy for the usage of dsDNA repair template, more importantly, the application of MDM2 antagonists provides a simple and efficient strategy to promote CRISPR/Cas9-mediated precise genome editing in sheep primary cells.

INTRODUCTION

The clustered regularly interspaced short palindromic repeats/CRISPR-associated protein 9 nuclease (CRISPR-Cas9) system has recently emerged as a powerful tool that allows targeted and efficient modification of eukaryotic genomes, which drives a revolution in biological research and holds immense promise to transform biotechnology, medicine, and agriculture.¹ This system is composed of a Cas9 endonuclease and a bifunctional single guide RNA (sgRNA),

which directs the Cas9 protein to the complementary target site located upstream of a requisite 5'-NGG protospacer adjacent motif (PAM) sequence. Binding of the PAM and a matching target then triggers Cas9 nuclease activity, leading to a site-specific genomic double-stranded break (DSB) in many eukaryotic organisms.²⁻⁴ The resulting DSB can be repaired by one of the two major DNA damage repair (DDR) pathways: the error-prone non-homologous end joining (NHEJ) or the error-free homology-directed repair (HDR) pathway. The NHEJ pathway generates stochastic insertions or deletions (indels) at the DSB, which is an effective and useful way of disrupting a gene of interest. However, NHEJ-mediated genome editing is not a reliable technique to generate precise genomic modifications because indels are unpredictable byproducts of it. Alternatively, the HDR pathway occurs in the presence of a homologous chromosome or exogenous DNA template at the DSB site, leading to precise deletions, insertions, or point mutations of interest. Such seamless modifications are desired for precise genome editing.⁵⁻⁸ Unfortunately, unlike NHEJ, which can operate throughout all phases of the cell cycle, HDR is largely restricted to late S and G2 phases when a sister chromatid is present, which can be used as the repair template to restore the lost genetic information.⁹ Moreover, NHEJ and HDR

Received 2 October 2021; accepted 31 December 2022;
<https://doi.org/10.1016/j.omtn.2022.12.020>

Correspondence: Shoulong Deng, NHC Key Laboratory of Human Disease Comparative Medicine, Institute of Laboratory Animal Sciences, Chinese Academy of Medical Sciences and Comparative Medicine Center, Peking Union Medical College, 5 Panjiayuananli, Chaoyang District, Beijing 100021, China.
E-mail: dengshoulong@cnilas.org

Correspondence: Xuguang Du, State Key Laboratory of Agrobiotechnology, College of Biological Sciences, China Agricultural University, Beijing 100193, China.
E-mail: xuguangdu@cau.edu.cn

Correspondence: Zhengxing Lian, Beijing Key Laboratory for Animal Genetic Improvement, National Engineering Laboratory for Animal Breeding, College of Animal Science and Technology, China Agricultural University, 2 Mingyuanxilu, Haidian District, Beijing 100193, China. .
E-mail: lianzhx@cau.edu.cn



are competing processes, and in most conditions, NHEJ usually triumphs over HDR. The efficiency of gene knockout mediated by CRISPR-Cas9 can now reach up to 100% in mammalian cells and embryos.^{10,11} By contrast, the efficiency for the CRISPR-Cas9-mediated precise introduction of an exogenous fragment varies widely between loci and cell types. For instance, in hematopoietic stem and progenitor cells (HSPCs), human pluripotent stem cells (hPSCs), and T cells, many groups achieved >40% of gene knockin efficiency.^{12–17} However, in some cell types, such as the primary fibroblasts, the HDR efficiency was typically quite low.^{8,18} Therefore, there is still a tremendous interest in further improving CRISPR-Cas9-mediated precise genome editing.

Multiple strategies have been developed to enhance the CRISPR-Cas9-mediated HDR efficiency. Genetic or chemical suppression of the key molecules in the NHEJ pathway such as *KU70*, *KU80*, and DNA ligase IV by short hairpin RNA (shRNA)-mediated gene silencing or inhibiting DNA-PKcs using small molecules has been shown to stimulate CRISPR-Cas9-mediated HDR.^{19–22} As an alternative strategy to inhibiting the NHEJ pathway, the administration of RS-1 or over-expression of *RAD51*, which is crucially involved in HDR, also had a considerable effect.^{23,24} In addition, several studies developed a high-throughput chemical screening platform to identify potential small molecules capable of enhancing precise genome editing, enabling an approximately 3-fold increase of efficiency for large fragment insertions and point mutations.^{25,26} Likewise, recent studies have identified that HDR could be enhanced by optimizing the design of the donor DNA template, particularly the use of single-stranded oligo DNA nucleotide (ssODN) rather than dsDNA as a donor template, or a double cut HDR donor, which is flanked by sgRNA-PAM sequences and is released after CRISPR-Cas9 cleavage.^{27,28} Moreover, other approaches such as the use of a targeted marker gene, use of NHEJ for integration, use of the Cas9-avidin/biotin-donor DNA system, and over-expression of a key gene that regulates apoptosis also enable precise genetic modifications to be achieved more efficiently.^{29–32}

Sheep are one of the most economically important forms of livestock, offering various high-quality products. Beyond wool, meat, and milk, genetically modified sheep have often been chosen as a large animal model in biomedical research due to their anatomy, physiology, and immunology being similar to those of humans, including for human vaccine development, asthma pathogenesis and treatment, the study of neonatal development, and the optimization of drug delivery and surgical techniques.³³ In this study, we intended to select *MSTN* and *FGF5* as target genes to conduct in-depth studies on CRISPR-Cas9-mediated genome editing due to their significance for affecting muscle and wool of sheep. *MSTN* is a member of the transforming growth factor β (TGF- β) superfamily that negatively regulates muscle mass. Naturally and manually induced mutations of *MSTN* cause an approximately 20% increase of muscle mass in many species, such as cattle,³⁴ dog,³⁵ and mice.³⁶ *FGF5* is a member of the fibroblast growth factor (FGF) superfamily that negatively regulates hair growth. Naturally occurring *FGF5* mutations in cat,³⁷ donkey,³⁸ and human³⁹ have

been shown to cause a pronounced increase in hair growth. Although the CRISPR-Cas9 system has recently provided a robust approach for sequence-specific gene knockout through NHEJ in the sheep genome, for the HDR-mediated precise manipulation of the sheep genome, there is a problem of inefficiency to be overcome,⁴⁰ limiting the development of sheep breeding and the application of sheep models for human disease research. Therefore, in this study, to enhance HDR, enabling more efficient precise genome editing in sheep fetal fibroblasts (SFFs), which are the major nuclear donors in the generation of genetically modified cloned sheep through somatic cell nuclear transfer (SCNT),⁴¹ we optimized several key parameters that affect HDR, such as the homology arm (HA) length and the amount of dsDNA repair template; we also assessed the impact of cell-cycle stage on HDR. Moreover, we tested three potent small molecules, RITA, Nutlin3, and CTX1, antagonists of the E3 ubiquitin ligase MDM2, which binds to the N-terminal transactivation domain of p53, inhibiting p53 transcriptional activity, or targeting p53 for proteasome-mediated degradation.^{42,43} We found that treatment with these antagonists could activate the p53 pathway and improve HDR efficiency by up to 4.28-fold, providing a simple and efficient strategy for precise genome editing in SFFs.

RESULTS

Establishing an efficient transfection system and determining the cleavage efficiencies of *MSTN* and *FGF5* sgRNAs in SFFs

The low transfection efficiency of primary cells has always restricted genome editing research in large animals. In this study, to achieve higher transfection efficiency, we compared two different transfection strategies, lipofection and nucleofection. At 48 h after transfection with the pEGFP-N1 plasmid, the transfection efficiency of conventional lipofection of the SFFs was only $10.67\% \pm 0.15\%$ as determined by flow cytometry, while the efficiency of nucleofection was as much as $95.07\% \pm 0.29\%$ (Figures 1A and 1B). In addition, the viability of SFFs subjected to nucleofection did not show any significant difference compared with the lipofection group (Figure S1A). Thus, we chose the nucleofection method for the follow-up experiments.

In this study, for the third exon of the sheep *MSTN* and *FGF5* genes, we designed one sgRNA each (Figures 1C and 1D) and then cloned the two sgRNA sequences into the pX330 plasmid. After the SFFs had been nucleofected with the pX330-*MSTN* or pX330-*FGF5* plasmid, TA cloning and Sanger sequencing assays revealed that the mutation rates were 14.7% and 25% (Figures 1E, 1F, S1B, and S1C), respectively, suggesting that the designed *MSTN* and *FGF5* sgRNAs work well.

Optimizing conditions and identifying potential enhancers for efficient HDR in SFFs

We next aimed to optimize several key parameters that affect HDR, such as the HA length and the amount of repair template, for enhancement of HDR efficiency at the *MSTN* locus in SFFs. To evaluate the HDR efficiency, we constructed a fluorescent reporter knockin system in SFFs (Figure 2A). In brief, after 48 h of co-transfection (pX330-*MSTN* plasmid and *MSTN*-T2A-EGFP repair

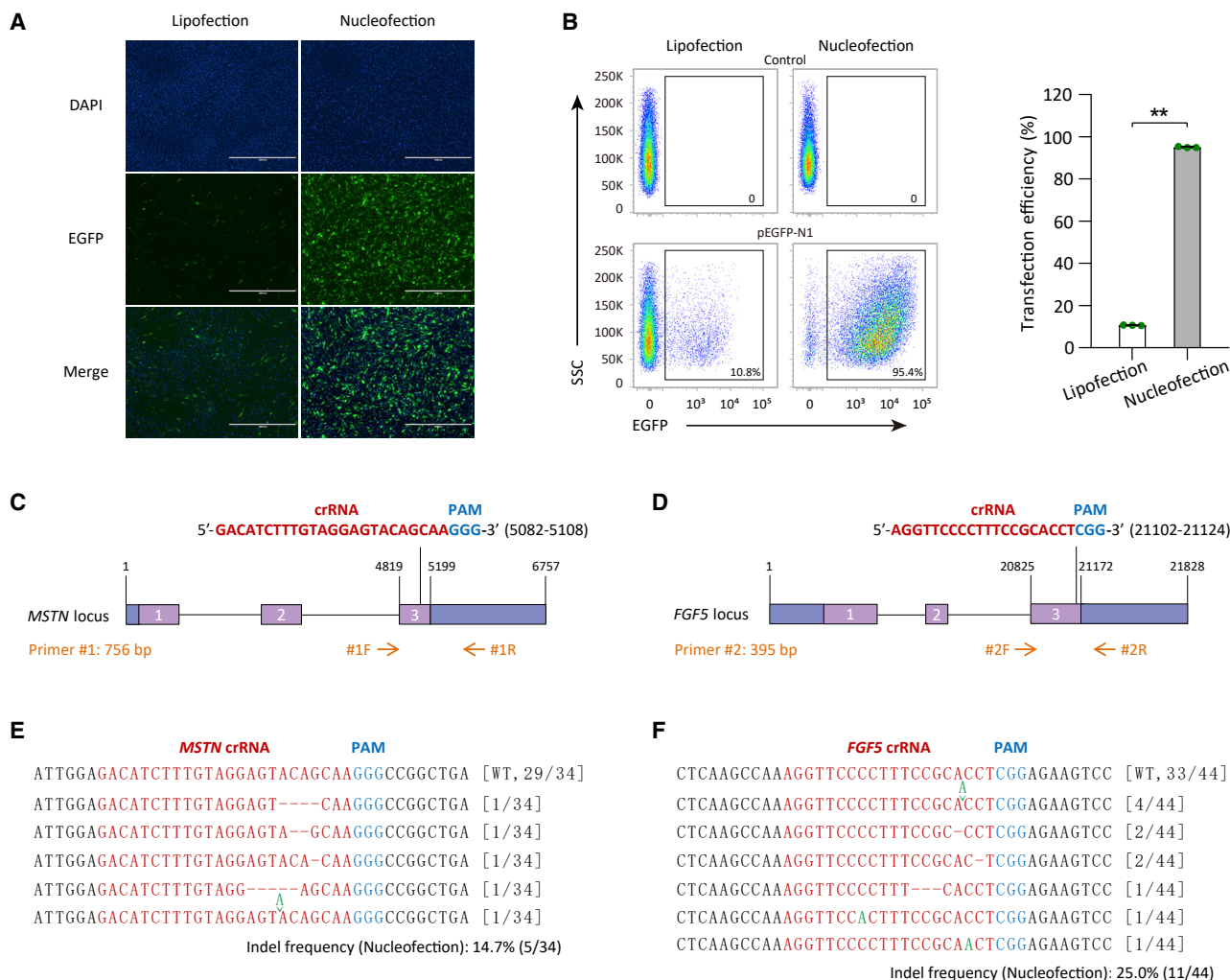


Figure 1. Establishing an efficient transfection system and determining the cleavage efficiencies of *MSTN* and *FGF5* sgRNAs in SFFs

(A) Fluorescence expression in SFFs transfected with the pEGFP-N1 plasmid by the indicated methods. (B) Determination of the efficiencies of lipofection and nucleofection by flow cytometry at 48 h post transfection. (C and D) Schematic of sgRNAs specific to exon 3 of the sheep *MSTN* and *FGF5* loci. The CRISPR RNA (crRNA) sequences are indicated in red typeface and the PAM in blue. Primers #1 and #2 were designed for PCR amplification of the region around the targeted sites to detect the indel frequencies of *MSTN* and *FGF5* genes, respectively. (E and F) TA cloning and Sanger sequencing analysis of the mutation types and efficiencies detected in the pX330-*MSTN* or pX330-*FGF5* plasmid-transfected SFFs. Deletions are indicated by a dashed line (–), and newly added nucleotides are highlighted in green. The colony numbers are surrounded by brackets.

template), sequencing results confirmed the correct integration of T2A-EGFP at the *MSTN* locus in SFFs (Figures 2B and S2A); flow cytometry results verified the effectiveness of the fluorescent reporter system. In other words, the EGFP⁺ cell population did not represent auto-fluorescent dead/dying cells (Figure S2C). What's more, while maintaining a constant amount of repair template (1 pmol), with the increase of HA from 50 to 500 bp, the HDR efficiency remained low, and a further increase to 750 and 1,000 bp led to significant increases in HDR efficiency (Figures 2C, 2D, and S2D), suggesting that a minimum HA length of 750 bp is required for efficient HDR in SFFs. While maintaining a constant HA length (500 bp), the HDR efficiency was not proportional to the amount of repair template. In

fact, the HDR efficiency initially elevated as the amount of repair template increased, with highest efficiency at 6 pmol, and then almost remained unchanged afterward (Figures 2E, 2F, and S2E), suggesting that the optimal amount of repair template is 6 pmol for efficient HDR in SFFs.

Besides optimization of the aforementioned conditions affecting HDR, we also sought to find a simple and efficient strategy to improve the HDR efficiency. Several small molecules have been reported as HDR-mediated precise genome editing enhancers through different mechanisms,^{21,24,25} such as SCR7. We thus investigated whether SCR7 has a notable effect in SFFs as well and tried novel small

molecules to enhance HDR efficiency. In this study, we investigated three kinds of potential enhancers, including chemical inhibitors of NHEJ (SCR7, PIK-75,⁴⁴ SF-2523,⁴⁵ CC-115⁴⁶), an inhibitor of p53 (pifithrin- β ^{47,48}), and several compounds, or cytokines that promote DDR (nicotinamide,⁴⁹ interleukin-10 [IL-10],⁵⁰ Ca²⁺⁵¹). We also used the T2A-EGFP system to evaluate the effect of the above-mentioned eight potential enhancers on CRISPR-Cas9-mediated HDR efficiency (Figure 2A). After transfection of the MSTN-T2A-EGFP with 1,000 bp HA (6 pmol) and the pX330-MSTN plasmid, varying concentrations of these eight potential enhancers were added into the culture medium. After 48 h of administration, flow cytometry analysis showed that the HDR efficiency in the presence of 10 μ M SCR7 was improved. However, nicotinamide, Ca²⁺, IL-10, SF2523, CC-115, and PIK-75 did not show significant improvement in HDR efficiency (Figures 2G, 2H, and S2F–S2H). Interestingly, the HDR efficiency had even declined remarkably when dealing with various concentrations of pifithrin- β (p53 inhibitor), suggesting that p53 may be functionally involved in the HDR pathway in SFFs.

MDM2 antagonists promote CRISPR-Cas9-mediated precise genome editing in SFFs

The HDR-weakening effect of p53 inhibitor aroused our curiosity, and we hypothesized that the activation of p53 could potentially improve HDR efficiency. To test this idea, we chose three small-molecule inhibitors of the p53-MDM2 interaction, including RITA, which binds the MDM2-interacting N terminus of p53 to prevent MDM2-mediated degradation, and Nutlin3 and CTX1, which directly bind MDM2 to prevent p53-MDM2 complex formation,^{42,43} and we used the T2A-EGFP system to conduct precise genome editing in SFFs at the *MSTN* and *FGF5* loci to investigate their effects on CRISPR-Cas9-mediated HDR (Figures 2A and 3A). First, we determined the cell viability of the pX330-MSTN plasmid and MSTN-T2A-EGFP with 1,000 bp HA repair template-transfected SFFs after exposure to different concentrations of RITA, Nutlin3, and CTX1 to assess the cytotoxicity of the three MDM2 antagonists. MTT results showed that Nutlin3 and CTX1 exhibited relatively mild cytotoxicity, and RITA demonstrated relatively severe cytotoxicity in high concentration (Figure S3A). Next, 10 μ M pifithrin- β , 10 nM RITA, 10 μ M Nutlin3, and 1.5 μ M CTX1 were added into the culture medium individually or in combination after SFFs were transfected with the pX330-MSTN/*FGF5* plasmid and MSTN/*FGF5*-T2A-EGFP with 1,000 bp HA repair template. qPCR was performed at 24 h post transfection to detect the mRNA levels of two key factors of the p53 pathway, including p21 (up-regulation) and Cdc25C (down-regulation),⁵² to examine whether the p53 pathway was activated in the Cas9/*MSTN* sgRNA/HDR/MDM2 antagonist-treated cells. The results showed that the expression level of p21 mRNA was obviously improved in RITA-, Nutlin3-, and CTX1-treated cells (Figure 3B), suggesting that the p53 pathway was activated upon MDM2 antagonist treatments in SFFs. Besides, as expected, Cdc25C mRNA expression was remarkably reduced in Nutlin3- and CTX1-treated cells, whereas RITA treatment slightly up-regulated Cdc25C mRNA expression in SFFs, which might result from these three molecules binding to different target sites and triggering different signal trans-

duction pathways. Furthermore, at 48 h post transfection, we observed that T2A-EGFP was precisely inserted into the *FGF5* locus in SFFs (Figures S2B and S3B). We also found that, similar to Figure 2H, flow cytometry results showed that pifithrin- β , the p53 inhibitor, decreased the efficiency of T2A-EGFP insertion by about 25% compared with that in DMSO-treated control cells at the *MSTN* and *FGF5* loci. Conversely, MDM2 antagonists significantly increased the efficiency of T2A-EGFP insertion in SFFs. In particular, treatment with the mixture of RITA, Nutlin3, and CTX1 greatly improved the HDR efficiency by 3.25-fold (Figures 3C–3F, S3C, and S3D). Meanwhile, we further performed karyotype analysis and whole-genome sequencing (WGS) in the Cas9/*MSTN* sgRNA/HDR/MDM2 antagonist-treated SFFs to detect the potential genotoxic activity of RITA, Nutlin3, and CTX1 and observed that the number (54), morphology, and integrity of chromosome were all normal (Figure S4A); the number of single-nucleotide polymorphisms (SNPs) and indels did not show obvious increase following treatments with RITA, Nutlin3, and CTX1 alone or the small-molecule mixture (Figure S4B). Collectively, these results suggest that MDM2 antagonists can promote HDR in SFFs without genotoxic effect.

MDM2 antagonists promote CRISPR-Cas9-mediated generation of knockin SFF lines

Encouraged by the HDR-enhancing effect of MDM2 antagonists, we applied them for the generation of mCherry knockin SFF lines without drug selection (Figure 4A). After nucleofection of the pX330-MSTN plasmid and CMV-mCherry-pA with the 1,000 bp HA donor template, SFFs were firstly incubated with RITA (10 nM) and Nutlin3 (10 μ M) for 48 h, then 576 single cells were picked up and cultured in 96-well plates with fresh medium. After 15 days of cell culture, we identified the occurrence of knockin at the *MSTN* locus by the observation of mCherry-positive single-cell colonies and genotyping (Figures 4C and 4D). DMSO-treated cells were used as control. We found that combined use of RITA and Nutlin3 could generate 7.45% of mCherry knockin SFF lines, and there was a 4.28-fold increase compared with the DMSO-treated group (1.74%). Interestingly, treatment with pifithrin- β (10 μ M), the inhibitor of p53, decreased the knockin efficiency (1.06%) once again (Figure 4B). These results suggest that MDM2 antagonists have a prominent application in the efficient generation of knockin SFF lines using the CRISPR-Cas9 system.

Effect of cell-cycle stage on HDR efficiency in SFFs

The tumor suppressor p53 is a powerful transcription factor that plays a central role in the regulation of cell cycle, which mainly determines the choice of the DSB repair pathway.^{8,53} In light of this, we next assessed whether treatment with MDM2 antagonists trigger cell-cycle arrest, as well as the effect of cell-cycle phase on CRISPR-Cas9-mediated HDR in SFFs. After co-transfection of the pX330-MSTN plasmid and MSTN-T2A-EGFP with the 1,000 bp HA donor template, SFFs were treated with 10 μ M pifithrin- β , 10 nM RITA, 10 μ M Nutlin3, and 1.5 μ M CTX1, respectively, and we analyzed the cell-cycle distribution by flow cytometry at 24 h post transfection. Compared with the mock group, treatment with MDM2 antagonists induced distinct G2/M phase arrest upon CRISPR-Cas9-mediated DNA damage in SFFs,

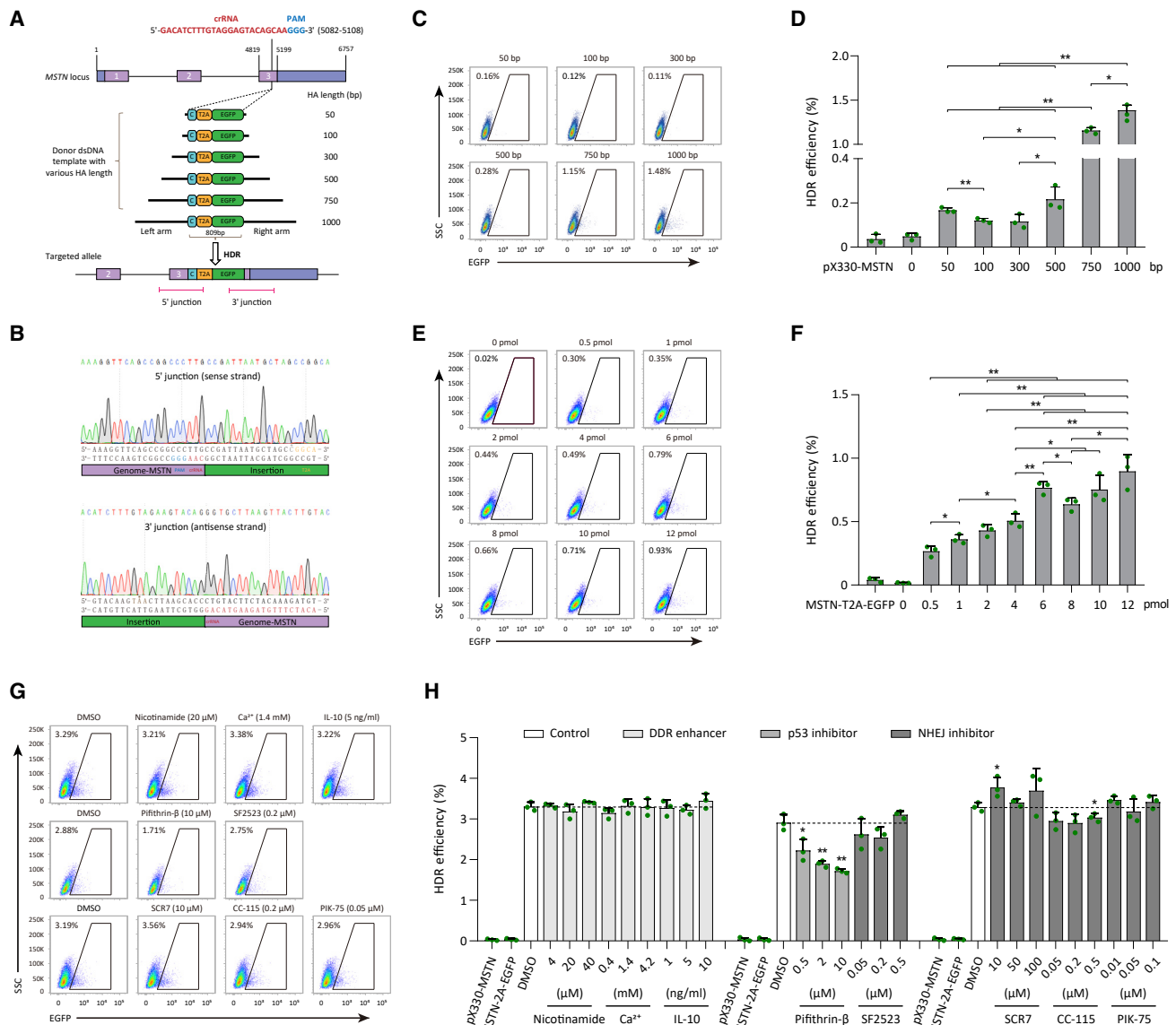
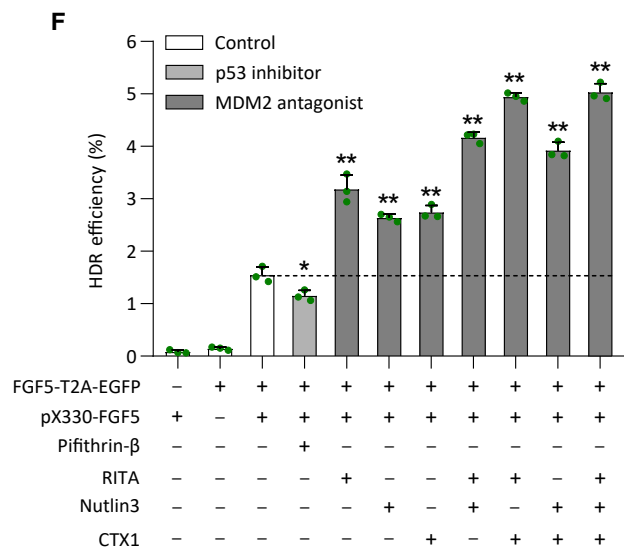
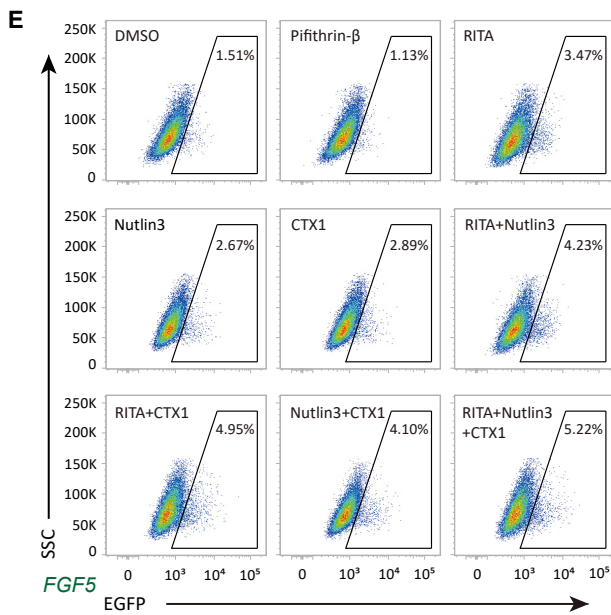
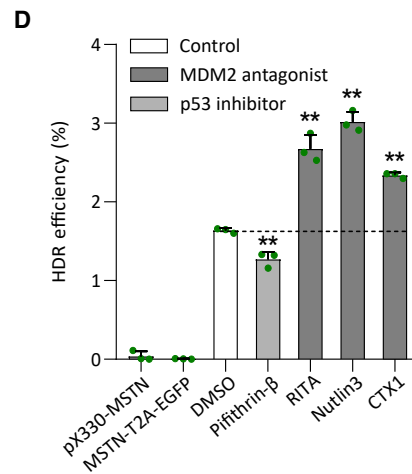
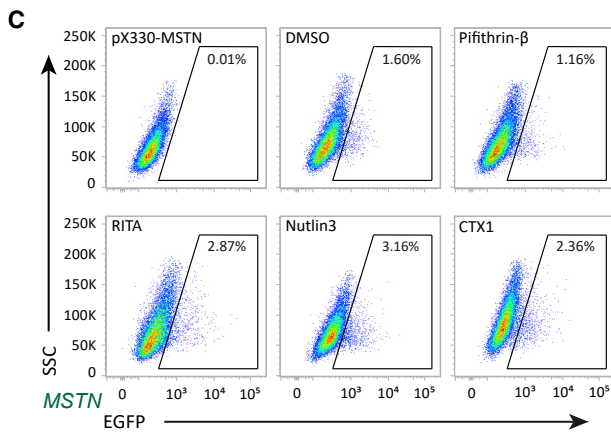
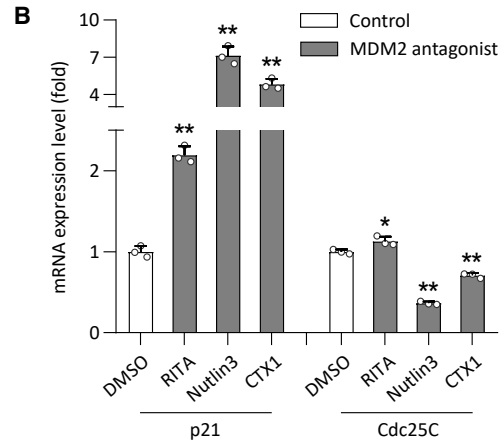
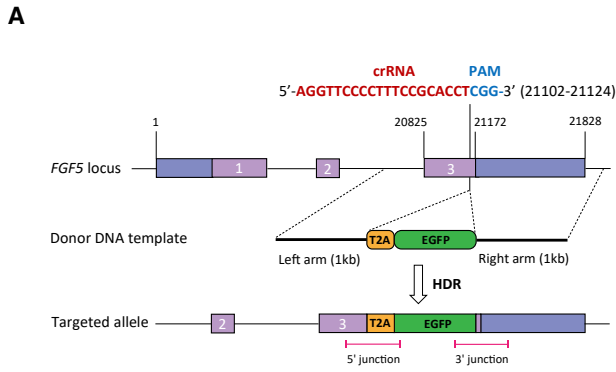


Figure 2. Optimizing conditions and identifying potential enhancers for efficient HDR in SFFs

(A) Schematic of the targeting strategy for knockin T2A-EGFP with HA in the length range of 50–1,000 bp to the sheep *MSTN* locus. The T2A-EGFP repair dsDNA templates were amplified from the *MSTN* donor plasmid by PCR. (B) Sanger sequencing of the 5' and 3' junction regions (T2A-EGFP) upon correct targeting at the *MSTN* locus. The intentionally added cytosine (C) is marked in gray, and the termination codon (TAA) of EGFP gene is marked in brown. (C) FACS analysis of EGFP-positive cells at 48 h after transfection of the pX330-MSTN plasmid and MSTN-T2A-EGFP with 50, 100, 300, 500, 750, or 1,000 bp HA repair template into SFFs. A representative FACS result of each length is shown. The cells transfected with the pX330-MSTN plasmid alone, or with MSTN-T2A-EGFP with the 0 bp HA repair template alone, were used as a negative control. (D) Effect of the HA length on HDR efficiency at the *MSTN* locus in SFFs. (E) FACS analysis of EGFP-positive cells at 48 h after transfection of the pX330-MSTN plasmid and different amounts of MSTN-T2A-EGFP with the 500 bp HA repair template into SFFs. A representative FACS result of each amount is shown. The cells transfected with the pX330-MSTN plasmid alone, or with MSTN-T2A-EGFP with the 500 bp HA repair template (1 pmol) alone, were used as a negative control. (F) Effect of the amount of repair template on HDR efficiency at the *MSTN* locus in SFFs. (G) FACS analysis of EGFP-positive cells at 48 h after transfection of the pX330-MSTN plasmid and MSTN-T2A-EGFP with 1,000 bp HA (6 pmol) into SFFs. Representative HDR efficiency of samples treated with 0.1% DMSO, 20 μ M nicotinamide, 1.4 mM Ca^{2+} , 5 ng/mL IL-10, 10 μ M pifithrin- β , 0.2 μ M SF2523, 10 μ M SCR7, 0.2 μ M CC-115, and 0.05 μ M PIK-75 are shown. DMSO-treated cells were used as a control. pX330-MSTN plasmid-transfected cells and MSTN-T2A-EGFP with the 1,000 bp HA repair template-transfected cells were used as negative control. (H) Effects of varying concentrations of different potential enhancers on HDR efficiency in SFFs. $n = 3$ biological replicates. Error bars represent SD. Significance was calculated using Tukey's multiple comparison test or Student's t test: * $p < 0.05$, ** $p < 0.01$.



(legend on next page)

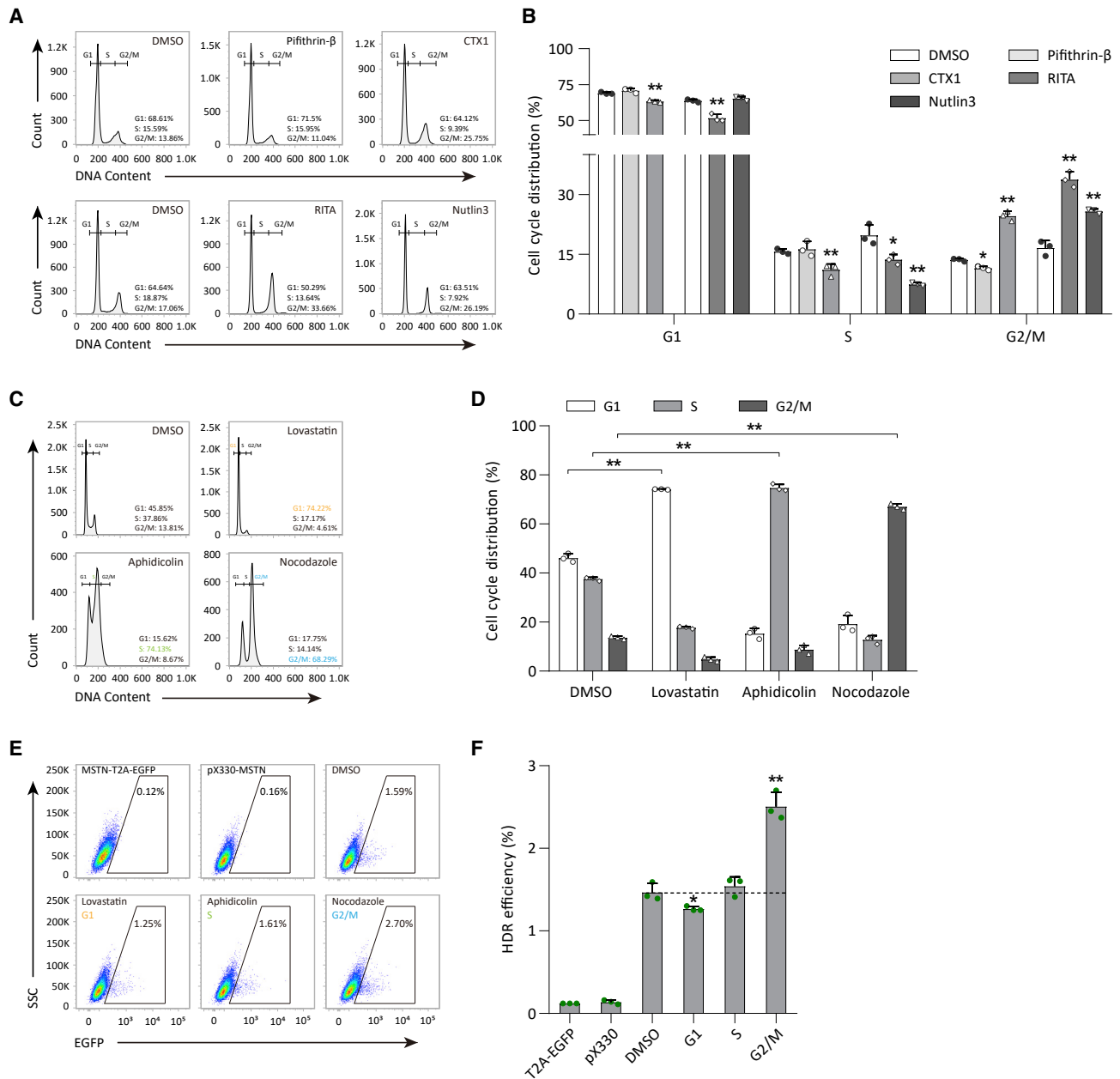


Figure 5. Effect of cell-cycle stage on HDR efficiency in SFFs

(A and B) Cell-cycle distribution of co-transfected SFFs after treatment with DMSO, 10 μ M pifithrin- β , 10 nM RITA, 10 μ M Nutlin3, and 1.5 μ M CTX1 for 24 h. Samples were stained by PI and analyzed by FACS. (C and D) Analysis of SFFs with different cell-cycle blocks by PI staining and flow cytometry. (E) FACS analysis of the HDR efficiency upon transfection with the pX330-MSTN plasmid and MSTN-T2A-EGFP with the 1,000 bp HA repair template into SFFs in different phases of the cell cycle. (F) Effects of different cell-cycle blocks on HDR efficiency. DMSO-treated cells served as a control. $n = 3$ biological replicates. Error bars represent SD. Significance was calculated using Student's t test: * $p < 0.05$, ** $p < 0.01$.

p53 mutation suppresses CRISPR-Cas9-mediated precise genome editing in SFFs

Higher HDR efficiency was achieved in the presence of MDM2 antagonists in wild-type SFFs. To further explore the HDR-enhancing effect of p53, we designed two sgRNAs targeting exons 1 and 3 of the

p53 gene to establish p53^{-/-} SFF lines (Figure 6A). We constructed two pX458 plasmids (pX458-p53-sgRNA1 and pX458-p53-sgRNA2) and transfected them into SFFs individually or in combination, and an approximately 493 bp deletion at the p53 locus would occur if the two sgRNAs worked well. A total of 576 EGFP-positive single cells

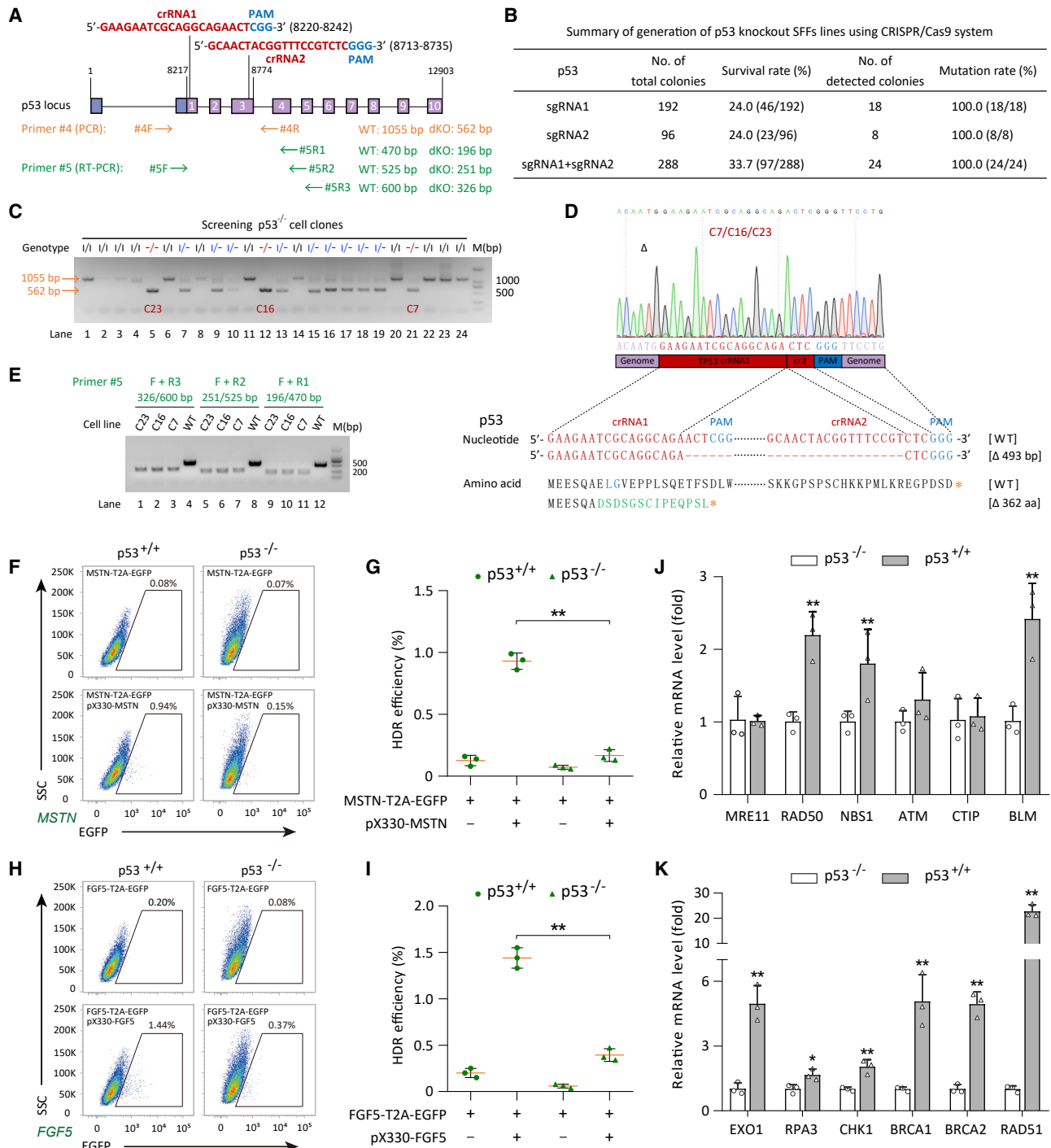


Figure 6. p53 mutation suppresses CRISPR-Cas9-mediated precise genome editing in SFFs

(A) Schematic diagram of the *p53* gene, with mutation in exons 1 and 3. The crRNA sequences are indicated in red typeface and the PAM in blue. The indels in the *p53* locus were detected by PCR (primer #4), and the predicted product sizes are 1,055 (wild type [WT]) and 562 bp (double knockout [dKO]). Primer #5 was designed for reverse transcription PCR (RT-PCR) to detect the mutation of p53 mRNA in SFFs. The predicted amplicon sizes are shown at the right side. (B) Summary of generation of p53 knockout SFF lines using the CRISPR-Cas9 system. sgRNA1 and sgRNA2 target exons 1 and 3 of the *p53* gene, respectively. (C) Genotyping results of *p53* gene knockout single-cell colonies selected in the sgRNA1 + sgRNA2-induced gene targeting using primer #4 (–, KO allele; I, whether this allele is mutated needs further verification by sequencing). Colonies with gene KO in at least one allele are marked in blue (I/–), and the biallelic mutation colonies are marked in red (–/–: C7, C16, and C23). (D) Sanger

(legend continued on next page)

were isolated by flow sorting from the three kinds of transfected cells, and 50 well-grown single-cell colonies were analyzed by PCR genotyping and Sanger sequencing (Figure 6B). Genotyping with primer #4 indicated that one 562 bp band was homozygous *p53* knockout colonies (C7, C16, and C23) and two bands (562 and 1,055 bp) were heterozygous colonies (Figure 6C). Since the anti-p53 antibody could not bind to the p53 protein extracted from wild-type SFFs (Figures S6A and S6B), the biallelic disruption at the *p53* locus in the three homozygotes colonies was further confirmed by Sanger sequencing and reverse transcription (RT)-PCR (Figures 6D and 6E). In addition, we determined by sequencing that all of the detected cell colonies contained mutations at the *p53* locus, suggesting that highly efficient gene knockout can be achieved by enrichment of genetically modified cells through flow sorting.

Having generated the *p53*^{-/-} SFF lines, we decided to assess whether the loss of p53 would affect the HDR efficiency. Accordingly, we compared the capacity of CRISPR-Cas9-mediated precise genome editing in same number of *p53*^{+/+} and *p53*^{-/-} SFFs by co-transfecting the pX330-MSTN plasmid and MSTN-T2A-EGFP with the 1,000 bp HA repair template. We first checked the cell viability by MTT assay after co-transfection and found that there was an obvious reduction in cell death in *p53*^{-/-} SFFs, which reconfirmed that p53 function was impaired in *p53*^{-/-} SFFs (Figure S6C). Furthermore, we observed that as expected, normal *p53*^{+/+} SFFs showed more efficient targeted knockin at the *MSTN* locus than *p53*^{-/-} SFFs (Figures 6F and 6G). Considering the heterogeneity of each locus, the effect of p53 loss on HDR was repeatedly assessed at another target site. Similar to the *MSTN* locus, FACS analysis showed that p53 loss resulted in 74% reduction in successful insertions at the *FGF5* locus (Figures 6H and 6I). In addition, we also detected the relative mRNA levels of 12 key regulatory genes involved in the HDR pathway between *p53*^{+/+} and *p53*^{-/-} SFFs and found that the expression of these genes were down-regulated in the *p53*^{-/-} SFFs compared with that in the *p53*^{+/+} SFFs. In particular, greater than 5-fold increases in *BRCA1*, *BRCA2*, and *RAD51* gene expression were observed in *p53*^{+/+} SFFs (Figures 6J and 6K). Taken together, these data indicate that p53 loss dramatically decreases the capacity of HDR in SFFs.

DISCUSSION

Precise genome editing mediated by HDR is of great utility in animal breeding and holds great promise for the generation of large-animal models of human disease. However, HDR efficiency is inherently low in some cell types, typically primary fibroblasts,^{54,55} which is one of the main barriers to engineering targeted modifications in their

genome via CRISPR-Cas9. The HDR efficiency is restricted by many factors, of which the structure of the repair template is one of the most crucial factors.^{28,56} Several studies have reported that the use of ssODN as the repair template exhibits higher HDR efficiency than dsDNA.^{27,57} However, such a strategy is limited to the introduction of short edits (<50 nt). In contrast, dsDNA is suitable for introducing large sequence changes and insertions, which broadens the range of applications. Hence, in this study, we focused on optimizing the use of dsDNA as the repair template. We first investigated the effect of HA length on the HDR efficiency due to its playing an important role in repair template design.⁵⁸ We found that increasing the HA length from 50 to 1,000 bp contributed to an increase in HDR efficiency, and we conclude that longer HA (>750 bp) is beneficial for precise genome editing in SFFs. In addition, increasing the amount of repair template did not lead to a sustained increase in HDR efficiency; thus, we identified the optimal amount of repair template (6 pmol) in SFFs. Together, these findings provide an optimized strategy for the usage of a dsDNA repair template to maximize HDR efficiency in SFFs.

The administration of small-molecule inhibitors or agonists has been shown to increase the efficiency of HDR-mediated precise genome editing in many mammalian cells.^{19–26} For example, by transient suppression of the key enzymes of the NHEJ pathway such as DNA ligase IV and DNA-PKcs through treatment with various inhibitors, DSB repair can be biased in favor of HDR. SCR7, an inhibitor of DNA ligase IV that targets the DNA-binding domain, increased the HDR efficiency by 1.8- to 19-fold in epithelial (A549) and melanoma (MelJuSo) cells.^{19,21} Similarly, NU7441, an inhibitor of DNA-PKcs that plays a critical role in initiating the NHEJ pathway, improved the HDR efficiency by 2- to 4-fold in human induced pluripotent stem cells (iPSCs) and HEK293T cells.^{20,22} Unfortunately, in our study, SCR7 only slightly increased the HDR efficiency by 14.7%; what's more, treatment with three novel DNA-PKcs inhibitors (PIK-75, SF-2523, and CC-115) did not appear to consistently enhance HDR in SFFs. Intriguingly, other studies also reported the unimpressive effects of DNA ligase IV (SCR7) and DNA-PKcs (NU7441 and NU7026) inhibitors on HDR in human iPSCs, mouse embryonic stem cells (ESCs), and rabbit embryos.^{24,28,59} Moreover, the opposite effect of small molecules on HDR can also be observed even under the same experimental condition. For example, the activation of CtIP, a core HDR factor, with MLN4924, which prevents its neddylation, resulted in HDR efficiency increases in human ESCs and iPSCs, whereas it decreased HDR efficiency in non-pluripotent human cells, such as immortalized cell lines (HEK293 and K562)

sequencing analysis of the three screened *p53*^{-/-} colonies. Nucleotide deletions are indicated by a dashed line (–). (E) RT-PCR results of the WT, C7, C16, and C23 cell lines using primer #5. (F and G) Determination of the HDR efficiency by flow cytometry at the *MSTN* locus in *p53*^{+/+} and *p53*^{-/-} SFFs at 48 h after transfection of the pX330-MSTN plasmid and MSTN-T2A-EGFP with the 1,000 bp HA repair template. The *MSTN* donor-transfected cells were used as a negative control. (H and I) Determination of the HDR efficiency by flow cytometry at the *FGF5* locus in *p53*^{+/+} and *p53*^{-/-} SFFs at 48 h after transfection of the pX330-FGF5 plasmid and FGF5-T2A-EGFP with the 1,000 bp HA repair template. The *FGF5* donor-transfected cells were used as a negative control. (J and K) Detection of the relative mRNA expression levels of the key regulatory genes involved in the HDR pathway at 24 h after transfection of the pX330-MSTN plasmid and MSTN-T2A-EGFP with the 1,000 bp HA repair template in *p53*^{+/+} and *p53*^{-/-} SFFs. The data were normalized to β -actin, and *p53*^{-/-} SFFs were used as a control. n = 3 biological replicates. Error bars represent SD. Significance was calculated using Student's t test: *p < 0.05, **p < 0.01.

and primary cells (human epidermal keratinocytes [HEKa] and CD4⁺ T cells).²² Cell-type-specific reliance on different DSB repair pathways could be one explanation for the discrepancy between these studies,^{8,22,28,59} which suggests the necessity of screening robust small molecules for the enhancement of HDR in the specific cell type of interest. Thus, we continued to identify more specific and potent small molecules targeting other key elements of the DSB repair pathway that can enhance HDR in SFFs. Recently, two studies reported that p53 activation inhibits CRISPR-Cas9 engineering in human ESCs, iPSCs, and retinal pigment epithelium cells (RPE1).^{48,60} As such, we reasoned that p53 could be a potential target. In addition, due to p53 protein's expression level and transcriptional activity often being inhibited by E3 ubiquitin ligase MDM2, we therefore focused on assessing the effects of small molecules targeting the p53-MDM2 interaction on HDR in SFFs. Interestingly, after the administration of pifithrin- β , an inhibitor of p53 protein, the HDR efficiency kept decreasing instead of increasing. Conversely, treatment with RITA, Nutlin3, or CTX1 alone, which neutralizes MDM2 inhibition rescuing p53 activity, or the small molecule mixture consistently increased HDR efficiency by 1.43- to 4.28-fold in SFFs. Furthermore, *p53*^{+/+} SFFs showed more efficient HDR activity than *p53*^{-/-} SFFs at *MSTN* and *FGF5* loci, providing further evidence that p53 promotes HDR-mediated precise genome editing in SFFs.

HDR is a complex process and depends on many variables, such as the cell type, chromatin state of the target DNA, and cell cycle,⁸ of which the cell cycle largely determines the choice between HDR and NHEJ in the response to DSBs.⁶¹ It has been shown to significantly increase HDR efficiency by chemically synchronizing cells to arrest them in the G2/M phase followed by timed delivery of Cas9-guide RNA ribonucleoprotein (RNP) complexes.⁶² Generating a fusion protein of Cas9 linked to the N-terminal region of human geminin to control the presence of Cas9 protein during the G2/M phase of the cell cycle but its absence during the G1 phase also showed a similar promoting effect.^{63,64} HDR is also regulated by multiple genes.^{63,64} As the "guardian of the genome" involved in maintaining genomic stability, p53 exerts a crucial role in the DNA damage response.⁶⁵ However, the effect of p53's function on HDR remains controversial. Apart from the aforementioned two studies, which observed that mutation of the *p53* gene could enhance HDR in human ESCs, iPSCs, and RPE1 cells,^{48,60} recently, Schiroli et al. reported that transient inhibition of p53 also could increase HDR-mediated integration in human HSPCs.¹² Interestingly, some previous studies suggested that p53 mutation did not impact HDR in mouse pancreatic cells and T lymphocytes⁶⁶ and a human pre-B cell line (Nalm-6).⁶⁷ And in this study, we found that *p53* gene knockout suppressed CRISPR-Cas9-mediated HDR in sheep fibroblasts. This discrepancy calls attention to the possibility that the impact of p53 on HDR is cell-type specific. Alternatively, several studies revealed that different types of mutations in the *p53* gene (e.g., null versus a point mutation) have different effects on HDR,⁶⁶ which may be another explanation for the discrepancy. The complex relationship between p53 and HDR deserves further investigation. Regardless of the discrepancy, after DSB formation, p53 controls the G2/M cell-cycle checkpoint and

mediates reversible growth arrest, which is thought to provide time for activating either the NHEJ or the HDR pathway to complete DNA DSB repair, thus preventing mutations from being propagated through DNA replication and mitosis.^{68,69} In the HDR pathway, DSB can be recognized by the MRE11/RAD50/NBS1 (MRN) complex, which recruits and activates ATM to phosphorylate the MRN-interacting protein CTIP and BRCA1, thereby triggering the initiation of DNA end resection, followed by removing nucleotides at the 5' ends near DSBs and generating 3' overhangs of single-stranded DNA (ssDNA) on both sides of DSB. After resection, these nascent ssDNAs are coated and stabilized by the RPA complex induced by exonuclease 1 (EXO1) and BLM helicase. Subsequently, RAD51 is phosphorylated by CHK1, resulting in the displacement of RPA from the 3' ssDNA overhangs and assembly of RAD51 nucleoprotein filaments mediated by BRCA2 and then searching for homologous donor DNA to achieve strand invasion.^{6,70,71} Our results indicate that treatment with inhibitors of the p53-MDM2 interaction further delay cell-cycle progression, causing G2/M cell-cycle arrest where HDR is observed to be most active, which contributes to increasing the HDR efficiency in SFFs. Moreover, almost all the key factors involved in the HDR pathway are highly suppressed in the absence of p53, which may explain why p53 is shown to enhance HDR-mediated precise genome editing in the sheep primary somatic cells.

In brief, our study optimized two key parameters in the use of dsDNA as the repair template and identified three potent small molecules to improve HDR efficiency in sheep primary cells. Yet, it is worth noting that some studies revealed that RITA (2 μ M) and Nutlin3 (20 μ M) could induce DNA damage in human and mouse cancer cell lines (HCT116, H460, and AJ02-NM0), characterized by the phosphorylation of H2A.X at Ser-139 and RPA32 at Ser-33 to form γ H2A.X and RPA32pS33 (DNA damage markers),^{42,72} which may lead to genomic mutations/instability. In light of this, we further examined the integrity of the genome of the CRISPR-Cas9-engineered sheep primary cells through karyotype analysis and WGS and observed that RITA, Nutlin3, and CTX1 treatments did not cause obvious genomic mutations/instability. Maybe the adverse/non-adverse effects of these small molecules are cell-type and drug-concentration dependent. In summary, this study provides a simple, efficient, and safe strategy to promote CRISPR-Cas9-mediated precise genome editing in sheep primary cells, which may contribute to the application of CRISPR-Cas9-engineered sheep in agricultural and biomedical research.

MATERIALS AND METHODS

Plasmid construction

The Cas9 and U6-sgRNA co-expression vector backbones pX330 and pX458 were purchased from Addgene (plasmid ID: 42230 and 48138). Sheep *MSTN*, *FGF5*, and p53 sgRNAs were designed using CRISPR Design Tool (<http://tools.genome-engineering.org>). To avoid targeting the conserved sequences of the TGF- β and FGF super-families, *MSTN* and *FGF5* sgRNAs were designed in the third exon of the sheep *MSTN* and *FGF5* genes. Four sgRNAs were used in this study: *MSTN* sgRNA (gacatctttgttaggagtacagca), *FGF5* sgRNA (aggttcccccttccgacct), p53 sgRNA1 (gaagaatcgcaggcagaact), and

p53 sgRNA2 (gcaactacggttcctctc). Two complementary guide sequence oligos were synthesized, annealed, and cloned into the pX330 or pX458 backbone vector to form the functional co-expression plasmids.⁷³

To construct donor plasmid for the sheep *MSTN* gene, 1 kb left and right HAs were amplified from the sheep genome by PCR and cloned into the pUC57 vector. The T2A-EGFP sequence (a cytosine was intentionally added ahead of the T2A sequence to ensure the correct reading frame at the *MSTN* locus) and the CMV-mCherry-pA sequence were subsequently inserted between the right and left HAs. The FGF5 donor plasmid also contained 1 kb left and right endogenous HAs and the T2A-EGFP exogenous sequence. For the *MSTN*/FGF5-T2A-EGFP fluorescent reporter knockin system, precise insertion resulted in fusion of *MSTN*/FGF5 and EGFP mediated by the T2A self-cleaving peptide, and the EGFP expression would be driven by the *MSTN*/FGF5 endogenous promoter.

Cell culture and transfection

SFFs were isolated from a 30-day-old Dorper fetus and cultured in Dulbecco's modified Eagle medium: Nutrient Mixture F-12 (DMEM/F12; Gibco) supplemented with 10% fetal bovine serum (FBS; Gibco) and 1% penicillin/streptomycin (Gibco) at 37°C with 5% CO₂.

The SFFs were transfected using lipofection or nucleofection. For lipofection, Lipofectamine 3000 Reagent (Invitrogen) was used in accordance with the manufacturer's instructions. For nucleofection, the Lonza Nucleofector 2b Device with Amaxa Basic Nucleofector Kit for Primary Fibroblasts (Lonza) was used as outlined in the manufacturer's instructions. In brief, the mixture of 1.5×10^6 SFFs and DNA was resuspended in 100 μ L nucleofector solution and nucleofected using program A-033. For the comparison of transfection efficiency experiment, 15 μ g pEGFP-N1 plasmid (Clontech) was used. For knockout experiments, 15 μ g individual plasmid (pX330-MSTN, pX330-FGF5, pX458-p53-sgRNA1, pX458-p53-sgRNA2) and mixed plasmid (pX458-p53-sgRNA1 + pX458-p53-sgRNA2) were used. For knockin experiments, pX330 plasmid and repair dsDNA template amplified from the donor plasmid were prepared as follows: 15 μ g pX330-MSTN and 1 pmol MSTN-T2A-EGFP with 50, 100, 300, 500, 750, and 1,000 bp HAs; 0.5, 1, 2, 4, 6, 8, 10, and 12 pmol MSTN-T2A-EGFP with 500 bp HA; 6 pmol MSTN-T2A-EGFP with 1,000 bp HA; 6 pmol MSTN-CMV-mCherry-pA with 1,000 bp HA; and 15 μ g pX330-FGF5 and 6 pmol FGF5-T2A-EGFP with 1,000 bp HA. After nucleofection, cells were transferred into 6-well plates for further culture and analysis.

HDR potential enhancers and MDM2 antagonist treatments

For *MSTN*/FGF5-T2A-EGFP knockin assays, co-transfected cells were treated with 0.1% DMSO (Sigma); 4, 20, and 40 μ M nicotinamide (Beyotime); 0.4, 1.4, and 4.2 mM Ca²⁺ (Sigma); 1, 5, and 10 ng/mL IL-10 (PeproTech); 0.5, 2, and 10 μ M pifithrin- β (MCE); 10, 50, and 100 μ M SCR7 (Selleck); 0.05, 0.2, and 0.5 μ M SF2523 (Selleck); 0.05, 0.2, and 0.5 μ M CC-115 (Selleck); 0.01, 0.05, and 0.1 μ M

PIK-75 (Selleck); 10 nM RITA (MCE); 10 μ M Nutlin3 (MCE); or 1.5 μ M CTX1 (MCE) for 48 h, followed by determining the HDR efficiency of each treatment through flow cytometry.

For cytotoxicity evaluation assay, co-transfected cells were treated with 0.1% DMSO; 2, 10, 15, and 30 nM RITA; 0.5, 2, 10, and 20 μ M Nutlin3; and 0.5, 1, 1.5, and 3 μ M CTX1 for 48 h, followed by measuring cell viability through MTT.

For detecting activation of p53 pathway, co-transfected cells were treated with 0.1% DMSO, 10 nM RITA, 10 μ M Nutlin3, and 1.5 μ M of CTX1 for 24 h, followed by determining the mRNA expression levels of p21 and Cdc25C by qPCR.

For CMV-mCherry-pA knockin assay, co-transfected cells were treated with 0.1% DMSO, 10 μ M pifithrin- β , and 10 nM RITA + 10 μ M Nutlin3 for 48 h, followed by picking single cells into 96-well plates.

For cell-cycle detection assay, co-transfected cells or wild-type cells were treated with 0.1% DMSO, 10 μ M pifithrin- β , 10 nM RITA, 10 μ M Nutlin3, or 1.5 μ M of CTX1 for 24 h, followed by analyzing cell-cycle distribution through flow cytometry.

Determination of indel frequency and PCR genotyping

For *MSTN* and *FGF5* gene knockout assays, primers #1 and #2 were used for PCR amplification of the region around the targeted sites to detect the indel frequencies, respectively. Genomic DNA was extracted using the Takara MiniBEST Universal Genomic DNA Extraction Kit in accordance with the manufacturer's instructions. With 10–50 ng DNA in 50 μ L reactions, the PCR amplification was performed using Q5 High-Fidelity DNA Polymerase (NEB), and PCR products with mutations were subcloned into a pEASY-Blunt Zero Cloning Vector (TransGen Biotech). Thirty-four (*MSTN*) and forty-four (*FGF5*) individual bacterial colonies from each sample were picked randomly for Sanger sequencing.

For CMV-mCherry-pA knockin assay, primer #3 was used for detection of on-target insertions. For *p53* gene knockout assay, primer #4 was used for detection of the *p53*^{-/-} SFF lines. In brief, part of each cell colony was lysed in lysis buffer containing 4% Tris-HCl (1 M, pH = 8.0), 0.9% Triton X-100, 0.9% NP-40, and 0.4 mg/mL proteinase K under the following conditions: 65°C for 30 min, followed by 95°C for 15 min, and held at 4°C. The lysate was directly used as template for PCR genotyping. PCR products were analyzed on a 1% agarose gel.

The detailed DNA sequences used for PCR primers are listed in [Table S1](#).

Determination of transfection/HDR efficiency and cell sorting

To evaluate the transfection efficiency and CRISPR-Cas9-mediated HDR efficiency, transfected cells were trypsinized and resuspended in 200 μ L PBS with 1% FBS. Data were acquired using a BD

FACSVerse flow cytometer. Live cells were gated using forward-scatter area and side-scatter area, and single cells were gated using forward-scatter width versus forward-scatter area.^{28,59,74} EGFP-positive cells were quantified by gating the appropriate channel using EGFP-negative cells as control. All of the flow cytometry data were analyzed with FlowJo (BD Biosciences).

For the generation of $p53^{-/-}$ cell lines, transfected cells were also trypsinized and resuspended, followed by sorting EGFP-positive single cells into 96-well plates using a BD FACSria III flow cytometer.

Karyotype analysis and WGS

For the karyotype analysis, the procedure has been described previously.⁷⁵ For the WGS, genomic DNA was extracted using the Takara MiniBEST Universal Genomic DNA Extraction Kit. Libraries were sequenced using the Novaseq platform (Illumina) at Allwegene, Beijing, China. Sheep reference genome assembly ARS-UI_Ramb_v2.0 was downloaded from NCBI. FastQC (v.0.11.9) was used to obtain clean reads. Burrows-Wheeler Alignment tool (BWA-v.0.7.17) and SAMtools (v0.1.19) were used to map reads to the reference genome with the command “mem -t 10 -M”. Picard was used to remove duplicated reads. Genome Analysis Toolkit (GATK-v.4.1.3.0) HaplotypeCaller, GenotypeGVCFs, and SelectVariants module were used to call variants. DMSO-1 sample was used as a control to count the SNPs and indels. All the WGS data have been deposited to Sequence Read Archive (SRA) at the National Center for Biotechnology Information (NCBI) under accession number NCBI: PRJNA905859.

Determination of cell viability and cell-cycle distribution

Cell viability was determined by MTT using the Cell Proliferation Kit I (Roche) in accordance with the manufacturer's instructions. Cell-cycle distributions were analyzed by flow cytometry after 24 h of exposure to pifithrin- β , RITA, Nutlin3, and CTX1, with or without co-transfection. In short, cells were harvested using 0.25% trypsin (Gibco) and fixed in cold 70% ethanol for 30 min, then washed twice with cold PBS, centrifuged at 2,000 RPM for 5 min, resuspended in 1 mg/mL RNase (Takara) with 50 μ g/mL propidium iodide (Sigma), and incubated for 30 min at 37°C. After incubation, cells were filtered through a 40 μ m cell strainer (Falcon) and analyzed on a BD FACSCalibur flow cytometer.

Cell-cycle synchronization

Before cell synchronization, it is important to ensure that SFFs are maintained at <70% confluence. Synchronization of cells in the G1 and G2/M phases were achieved by treatment with 40 μ M lovastatin (MCE) and 200 ng/mL nocodazole (MCE) for 17 h, respectively. Synchronization of cells in S phase required two sequential treatments: cells were first treated with 2 μ g/mL aphidicolin (Abcam) for 17 h, then released in aphidicolin-free medium for 4.5 h and again treated with a second dose of drugs for 17 h. DMSO was used as a control. After cell synchronization, cell-cycle distributions were analyzed by flow cytometry as described above.

Fluorescence microscopy

pEGFP-N1 plasmid-transfected cells and mCherry knockin SFFs (and negative control cells) were cultured in 6-well plates and 8-well glass chamber slides (Millipore), respectively. In brief, cells were fixed with 4% paraformaldehyde for 15 min at room temperature, followed by washing with PBS three times for 5 min each time and staining with DAPI (Beyotime) for 2 min at room temperature. Images were taken using a Nikon Eclipse Ti microscope (EGFP) and Nikon A1 confocal microscope (mCherry).

RT-PCR and quantitative real-time PCR

Total RNA was extracted using the RNeasy Micro kit (Qiagen) in accordance with the manufacturer's instructions. cDNA was synthesized using the PrimeScript RT reagent kit (Takara) following the manufacturer's protocol. β -Actin was used as a representative house-keeping gene for normalization. For the RT-PCR assay, primer #5 was used for detection of the mutation of p53 mRNA in SFFs. For the qPCR assay, each 20 μ L sample for the qPCR reaction contained 2 μ L cDNA, 0.4 μ M of both of the forward and reverse primers, 0.4 μ L Rox Reference Dye II, and 10 μ L SYBR Premix Ex Taq II (Takara). The qPCR reactions were run on the Mx3000P instrument (Agilent Technologies) with the following conditions: 95°C for 30 s, followed by 40 cycles of 95°C for 5 s, 60°C for 30 s, and 72°C for 30 s. The data were analyzed using Mx3000P software. The relative expression was determined using the comparative $2^{-\Delta\Delta CT}$ method.

The detailed DNA sequences used for RT-PCR and qPCR primers are listed in Table S1.

Statistical analysis

The data were analyzed by Student's t test or χ^2 test for comparisons between two groups and Tukey's multiple comparison test for multiple groups (SAS). All values are presented as mean \pm SD. The differences were considered statistically significant at * $p < 0.05$ and ** $p < 0.01$.

DATA AVAILABILITY

All data in this study are available under reasonable request; please contact lianzhx@cau.edu.cn.

SUPPLEMENTAL INFORMATION

Supplemental information can be found online at <https://doi.org/10.1016/j.omtn.2022.12.020>.

ACKNOWLEDGMENTS

We thank Ling Lian, Kun Yu, Tao Feng, Chunlong Xu, Pan Li, Yiming Yuan, and Zirun Tang for helpful discussions associated with the manuscript. This work was supported by the National Science and Technology Major Project of China (2016ZX08008-003); National Natural Science Foundation of China (32072721 and 32272853); National Key Research and Development Program (2021YFD1200900); and National Science and Technology Support Program (2015BAD03B05).

AUTHOR CONTRIBUTIONS

Z.L. designed the study. Yan Li, D.L., J.W., Y.Z., and Yao Li performed experiments, analyzed the data, and wrote the manuscript. S.D. and X.D. provided technical assistance. G.L. and S.W. provided valuable comments.

DECLARATION OF INTERESTS

The authors declare no competing interests.

REFERENCES

- Hsu, P.D., Lander, E.S., and Zhang, F. (2014). Development and applications of CRISPR-Cas9 for genome engineering. *Cell* 157, 1262–1278.
- Mali, P., Yang, L., Esvelt, K.M., Aach, J., Guell, M., DiCarlo, J.E., Norville, J.E., and Church, G.M. (2013). RNA-guided human genome engineering via Cas9. *Science* 339, 823–826.
- Cong, L., Ran, F.A., Cox, D., Lin, S., Barretto, R., Habib, N., Hsu, P.D., Wu, X., Jiang, W., Marraffini, L.A., and Zhang, F. (2013). Multiplex genome engineering using CRISPR/Cas systems. *Science* 339, 819–823.
- Jinek, M., Chylinski, K., Fonfara, I., Hauer, M., Doudna, J.A., and Charpentier, E. (2012). A programmable dual-RNA-guided DNA endonuclease in adaptive bacterial immunity. *Science* 337, 816–821.
- Sander, J.D., and Joung, J.K. (2014). CRISPR-Cas systems for editing, regulating and targeting genomes. *Nat. Biotechnol.* 32, 347–355.
- Ciccia, A., and Elledge, S.J. (2010). The DNA damage response: making it safe to play with knives. *Mol. Cell* 40, 179–204.
- Rees, H.A., and Liu, D.R. (2018). Base editing: precision chemistry on the genome and transcriptome of living cells. *Nat. Rev. Genet.* 19, 770–788.
- Komor, A.C., Badran, A.H., and Liu, D.R. (2017). CRISPR-based technologies for the manipulation of eukaryotic genomes. *Cell* 169, 559.
- Heyer, W.D., Ehmsen, K.T., and Liu, J. (2010). Regulation of homologous recombination in eukaryotes. *Annu. Rev. Genet.* 44, 113–139.
- Wang, H., Yang, H., Shivalila, C.S., Dawlaty, M.M., Cheng, A.W., Zhang, F., and Jaenisch, R. (2013). One-step generation of mice carrying mutations in multiple genes by CRISPR/Cas-mediated genome engineering. *Cell* 153, 910–918.
- Yang, H., Wang, H., Shivalila, C.S., Cheng, A.W., Shi, L., and Jaenisch, R. (2013). One-step generation of mice carrying reporter and conditional alleles by CRISPR/Cas-mediated genome engineering. *Cell* 154, 1370–1379.
- Schirotti, G., Conti, A., Ferrari, S., Della Volpe, L., Jacob, A., Albano, L., Beretta, S., Calabria, A., Vavassori, V., Gasparini, P., et al. (2019). Precise gene editing preserves hematopoietic stem cell function following transient p53-mediated DNA damage response. *Cell Stem Cell* 24, 551–565.e8.
- Suzuki, S., Crane, A.M., Anirudhan, V., Barilla, C., Matthias, N., Randell, S.H., Rab, A., Sorscher, E.J., Kerschner, J.L., Yin, S., et al. (2020). Highly efficient gene editing of cystic fibrosis patient-derived airway basal cells results in functional CFTR correction. *Mol. Ther.* 28, 1684–1695.
- Martin, R.M., Ikeda, K., Cromer, M.K., Uchida, N., Nishimura, T., Romano, R., Tong, A.J., Lemgart, V.T., Camarena, J., Pavel-Dinu, M., et al. (2019). Highly efficient and marker-free genome editing of human pluripotent stem cells by CRISPR-Cas9 RNP and AAV6 donor-mediated homologous recombination. *Cell Stem Cell* 24, 821–828.e5.
- Vaidyanathan, S., Salahudeen, A.A., Sellers, Z.M., Bravo, D.T., Choi, S.S., Batish, A., Le, W., Baik, R., de la O, S., Kaushik, M.P., et al. (2020). High-efficiency, selection-free gene repair in airway stem cells from cystic fibrosis patients rescues CFTR function in differentiated epithelia. *Cell Stem Cell* 26, 161–171.e4.
- Charlesworth, C.T., Camarena, J., Cromer, M.K., Vaidyanathan, S., Bak, R.O., Carte, J.M., Potter, J., Dever, D.P., and Porteus, M.H. (2018). Priming human repopulating hematopoietic stem and progenitor cells for Cas9/sgRNA gene targeting. *Mol. Ther. Nucleic Acids* 12, 89–104.
- Eyquem, J., Mansilla-Soto, J., Giavridis, T., van der Stegen, S.J.C., Hamieh, M., Cunanan, K.M., Odak, A., Gönen, M., and Sadelain, M. (2017). Targeting a CAR to the TRAC locus with CRISPR/Cas9 enhances tumour rejection. *Nature* 543, 113–117.
- Li, P., Zhang, L., Li, Z., Xu, C., Du, X., and Wu, S. (2020). Cas12a mediates efficient and precise endogenous gene tagging via MITI: microhomology-dependent targeted integrations. *Cell. Mol. Life Sci.* 77, 3875–3884.
- Chu, V.T., Weber, T., Wefers, B., Wurst, W., Sander, S., Rajewsky, K., and Kühn, R. (2015). Increasing the efficiency of homology-directed repair for CRISPR-Cas9-induced precise gene editing in mammalian cells. *Nat. Biotechnol.* 33, 543–548.
- Robert, F., Barbeau, M., Éthier, S., Dostie, J., and Pelletier, J. (2015). Pharmacological inhibition of DNA-PK stimulates Cas9-mediated genome editing. *Genome Med.* 7, 93.
- Maruyama, T., Dougan, S.K., Truttmann, M.C., Bilate, A.M., Ingram, J.R., and Ploegh, H.L. (2015). Increasing the efficiency of precise genome editing with CRISPR-Cas9 by inhibition of nonhomologous end joining. *Nat. Biotechnol.* 33, 538–542.
- Riesenberg, S., and Maricic, T. (2018). Targeting repair pathways with small molecules increases precise genome editing in pluripotent stem cells. *Nat. Commun.* 9, 2164.
- Pinder, J., Salsman, J., and Dellaire, G. (2015). Nuclear domain 'knock-in' screen for the evaluation and identification of small molecule enhancers of CRISPR-based genome editing. *Nucleic Acids Res.* 43, 9379–9392.
- Song, J., Yang, D., Xu, J., Zhu, T., Chen, Y.E., and Zhang, J. (2016). RS-1 enhances CRISPR/Cas9- and TALEN-mediated knock-in efficiency. *Nat. Commun.* 7, 10548.
- Yu, C., Liu, Y., Ma, T., Liu, K., Xu, S., Zhang, Y., Liu, H., La Russa, M., Xie, M., Ding, S., and Qi, L.S. (2015). Small molecules enhance CRISPR genome editing in pluripotent stem cells. *Cell Stem Cell* 16, 142–147.
- Ma, X., Chen, X., Jin, Y., Ge, W., Wang, W., Kong, L., Ji, J., Guo, X., Huang, J., Feng, X.H., et al. (2018). Small molecules promote CRISPR-Cpf1-mediated genome editing in human pluripotent stem cells. *Nat. Commun.* 9, 1303.
- Richardson, C.D., Ray, G.J., DeWitt, M.A., Curie, G.L., and Corn, J.E. (2016). Enhancing homology-directed genome editing by catalytically active and inactive CRISPR-Cas9 using asymmetric donor DNA. *Nat. Biotechnol.* 34, 339–344.
- Zhang, J.P., Li, X.L., Li, G.H., Chen, W., Arakaki, C., Botimer, G.D., Baylink, D., Zhang, L., Wen, W., Fu, Y.W., et al. (2017). Efficient precise knockin with a double cut HDR donor after CRISPR/Cas9-mediated double-stranded DNA cleavage. *Genome Biol.* 18, 35.
- Dever, D.P., Bak, R.O., Reinisch, A., Camarena, J., Washington, G., Nicolas, C.E., Pavel-Dinu, M., Saxena, N., Wilkens, A.B., Mantri, S., et al. (2016). CRISPR/Cas9 β -globin gene targeting in human haematopoietic stem cells. *Nature* 539, 384–389.
- Suzuki, K., Tsunekawa, Y., Hernandez-Benitez, R., Wu, J., Zhu, J., Kim, E.J., Hatanaka, F., Yamamoto, M., Araoka, T., Li, Z., et al. (2016). In vivo genome editing via CRISPR/Cas9 mediated homology-independent targeted integration. *Nature* 540, 144–149.
- Ma, M., Zhuang, F., Hu, X., Wang, B., Wen, X.Z., Ji, J.F., and Xi, J.J. (2017). Efficient generation of mice carrying homozygous double-loxP alleles using the Cas9-Avidin/Biotin-donor DNA system. *Cell Res.* 27, 578–581.
- Li, X.L., Li, G.H., Fu, J., Fu, Y.W., Zhang, L., Chen, W., Arakaki, C., Zhang, J.P., Wen, W., Zhao, M., et al. (2018). Highly efficient genome editing via CRISPR-Cas9 in human pluripotent stem cells is achieved by transient BCL-XL overexpression. *Nucleic Acids Res.* 46, 10195–10215.
- Scheerlinck, J.P.Y., Snibson, K.J., Bowles, V.M., and Sutton, P. (2008). Biomedical applications of sheep models: from asthma to vaccines. *Trends Biotechnol.* 26, 259–266.
- Luo, J., Song, Z., Yu, S., Cui, D., Wang, B., Ding, F., Li, S., Dai, Y., and Li, N. (2014). Efficient generation of myostatin (MSTN) biallelic mutations in cattle using zinc finger nucleases. *PLoS One* 9, e95225.
- Zou, Q., Wang, X., Liu, Y., Ouyang, Z., Long, H., Wei, S., Xin, J., Zhao, B., Lai, S., Shen, J., et al. (2015). Generation of gene-target dogs using CRISPR/Cas9 system. *J. Mol. Cell Biol.* 7, 580–583.
- Lee, S.J., and McPherron, A.C. (2001). Regulation of myostatin activity and muscle growth. *Proc. Natl. Acad. Sci. USA* 98, 9306–9311.
- Drögemüller, C., Rüfenacht, S., Wichert, B., and Leeb, T. (2007). Mutations within the FGF5 gene are associated with hair length in cats. *Anim. Genet.* 38, 218–221.

38. Legrand, R., Tiret, L., and Abitbol, M. (2014). Two recessive mutations in FGF5 are associated with the long-hair phenotype in donkeys. *Genet. Sel. Evol.* 46, 65.
39. Higgins, C.A., Petukhova, L., Harel, S., Ho, Y.Y., Drill, E., Shapiro, L., Wajid, M., and Christiano, A.M. (2014). FGF5 is a crucial regulator of hair length in humans. *Proc. Natl. Acad. Sci. USA* 111, 10648–10653.
40. Menchaca, A., Anegón, I., Whitelaw, C.B.A., Baldassarre, H., and Crispo, M. (2016). New insights and current tools for genetically engineered (GE) sheep and goats. *Theriogenology* 86, 160–169.
41. Schnieke, A.E., Kind, A.J., Ritchie, W.A., Mycock, K., Scott, A.R., Ritchie, M., Wilmut, I., Colman, A., and Campbell, K.H. (1997). Human factor IX transgenic sheep produced by transfer of nuclei from transfected fetal fibroblasts. *Science* 278, 2130–2133.
42. Wanzel, M., Vischedyk, J.B., Gittler, M.P., Gremke, N., Seiz, J.R., Hefter, M., Noack, M., Savai, R., Mernberger, M., Charles, J.P., et al. (2016). CRISPR-Cas9–based target validation for p53-reactivating model compounds. *Nat. Chem. Biol.* 12, 22–28.
43. Karan, G., Wang, H., Chakrabarti, A., Karan, S., Liu, Z., Xia, Z., Gundluru, M., Moreton, S., Sauntharajah, Y., Jackson, M.W., et al. (2016). Identification of a small molecule that overcomes HdmX-mediated suppression of p53. *Mol. Cancer Ther.* 15, 574–582.
44. Graham, T.G.W., Walter, J.C., and Loparo, J.J. (2016). Two-stage synapsis of DNA ends during non-homologous end joining. *Mol. Cell* 61, 850–858.
45. Carlino, L., and Rastelli, G. (2016). Dual kinase-bromodomain inhibitors in anti-cancer drug discovery: a structural and pharmacological perspective. *J. Med. Chem.* 59, 9305–9320.
46. Mortensen, D.S., Perrin-Ninkovic, S.M., Shevlin, G., Elsner, J., Zhao, J., Whitefield, B., Tehrani, L., Sapienza, J., Riggs, J.R., Parnes, J.S., et al. (2015). Optimization of a series of triazole containing mammalian target of rapamycin (mTOR) kinase inhibitors and the discovery of CC-115. *J. Med. Chem.* 58, 5599–5608.
47. Walton, M.I., Wilson, S.C., Hardcastle, I.R., Mirza, A.R., and Workman, P. (2005). An evaluation of the ability of pifithrin- α and - β to inhibit p53 function in two wild-type p53 human tumor cell lines. *Mol. Cancer Ther.* 4, 1369–1377.
48. Haapaniemi, E., Botla, S., Persson, J., Schmierer, B., and Taipale, J. (2018). CRISPR-Cas9 genome editing induces a p53-mediated DNA damage response. *Nat. Med.* 24, 927–930.
49. Surjana, D., Halliday, G.M., and Damian, D.L. (2010). Role of Nicotinamide in DNA damage, mutagenesis, and DNA repair. *J. Nucleic Acids* 2010, 157591.
50. Nishigori, C., Yarosh, D.B., Ullrich, S.E., Vink, A.A., Bucana, C.D., Roza, L., and Kripke, M.L. (1996). Evidence that DNA damage triggers interleukin 10 cytokine production in UV-irradiated murine keratinocytes. *Proc. Natl. Acad. Sci. USA* 93, 10354–10359.
51. Bugreev, D.V., and Mazin, A.V. (2004). Ca²⁺ activates human homologous recombination protein Rad51 by modulating its ATPase activity. *Proc. Natl. Acad. Sci. USA* 101, 9988–9993.
52. Giono, L.E., Resnick-Silverman, L., Carvajal, L.A., St Clair, S., and Manfredi, J.J. (2017). Mdm2 promotes Cdc25C protein degradation and delays cell cycle progression through the G2/M phase. *Oncogene* 36, 6762–6773.
53. Shangary, S., and Wang, S. (2008). Targeting the MDM2-p53 interaction for cancer therapy. *Clin. Cancer Res.* 14, 5318–5324.
54. Kass, E.M., Helgadottir, H.R., Chen, C.C., Barbera, M., Wang, R., Westermarck, U.K., Ludwig, T., Moynahan, M.E., and Jasin, M. (2013). Double-strand break repair by homologous recombination in primary mouse somatic cells requires BRCA1 but not the ATM kinase. *Proc. Natl. Acad. Sci. USA* 110, 5564–5569.
55. Li, G., Liu, D., Zhang, X., Quan, R., Zhong, C., Mo, J., Huang, Y., Wang, H., Ruan, X., Xu, Z., et al. (2018). Suppressing Ku70/Ku80 expression elevates homology-directed repair efficiency in primary fibroblasts. *Int. J. Biochem. Cell Biol.* 99, 154–160.
56. Yao, X., Zhang, M., Wang, X., Ying, W., Hu, X., Dai, P., Meng, F., Shi, L., Sun, Y., Yao, N., et al. (2018). Tild-CRISPR allows for efficient and precise gene knockin in mouse and human cells. *Dev. Cell* 45, 526–536.e5.
57. Yang, L., Guell, M., Byrne, S., Yang, J.L., De Los Angeles, A., Mali, P., Aach, J., Kim-Kiselak, C., Briggs, A.W., Rios, X., et al. (2013). Optimization of scarless human stem cell genome editing. *Nucleic Acids Res.* 41, 9049–9061.
58. Paix, A., Folkmann, A., Goldman, D.H., Kulaga, H., Grzelak, M.J., Rasoloson, D., Paidemarry, S., Green, R., Reed, R.R., and Seydoux, G. (2017). Precision genome editing using synthesis-dependent repair of Cas9-induced DNA breaks. *Proc. Natl. Acad. Sci. USA* 114, E10745–E10754.
59. Shy, B.R., MacDougall, M.S., Clarke, R., and Merrill, B.J. (2016). Co-incident insertion enables high efficiency genome engineering in mouse embryonic stem cells. *Nucleic Acids Res.* 44, 7997–8010.
60. Ihry, R.J., Worringer, K.A., Salick, M.R., Frias, E., Ho, D., Theriault, K., Kommineni, S., Chen, J., Sondey, M., Ye, C., et al. (2018). p53 inhibits CRISPR-Cas9 engineering in human pluripotent stem cells. *Nat. Med.* 24, 939–946.
61. Orthwein, A., Noordermeer, S.M., Wilson, M.D., Landry, S., Enchev, R.I., Sherker, A., Munro, M., Pinder, J., Salsman, J., Dellaire, G., et al. (2015). A mechanism for the suppression of homologous recombination in G1 cells. *Nature* 528, 422–426.
62. Lin, S., Staahl, B.T., Alla, R.K., and Doudna, J.A. (2014). Enhanced homology-directed human genome engineering by controlled timing of CRISPR/Cas9 delivery. *Elife* 3, e04766.
63. Gutschner, T., Haemmerle, M., Genovese, G., Draetta, G.F., and Chin, L. (2016). Post-translational regulation of Cas9 during G1 enhances homology-directed repair. *Cell Rep.* 14, 1555–1566.
64. Howden, S.E., McColl, B., Glaser, A., Vadolas, J., Petrou, S., Little, M.H., Elefanty, A.G., and Stanley, E.G. (2016). A Cas9 variant for efficient generation of indel-free knockin or gene-corrected human pluripotent stem cells. *Stem Cell Rep.* 7, 508–517.
65. Kim, J., Yu, L., Chen, W., Xu, Y., Wu, M., Todorova, D., Tang, Q., Feng, B., Jiang, L., He, J., et al. (2019). Wild-type p53 promotes cancer metabolic switch by inducing PUMA-dependent suppression of oxidative phosphorylation. *Cancer Cell* 35, 191–203.e8.
66. Wiktor-Brown, D.M., Sukup-Jackson, M.R., Fakhraldeen, S.A., Hendricks, C.A., and Engelward, B.P. (2011). p53 null fluorescent yellow direct repeat (FYDR) mice have normal levels of homologous recombination. *DNA Repair* 10, 1294–1299.
67. So, S., Adachi, N., and Koyama, H. (2007). Absence of p53 enhances growth defects and etoposide sensitivity of human cells lacking the bloom syndrome helicase BLM. *DNA Cell Biol.* 26, 517–525.
68. Bunz, F., Dutriaux, A., Lengauer, C., Waldman, T., Zhou, S., Brown, J.P., Sedivy, J.M., Kinzler, K.W., and Vogelstein, B. (1998). Requirement for p53 and p21 to sustain G2 arrest after DNA damage. *Science* 282, 1497–1501.
69. Khanna, K.K., and Jackson, S.P. (2001). DNA double-strand breaks: signaling, repair and the cancer connection. *Nat. Genet.* 27, 247–254.
70. Blackford, A.N., and Jackson, S.P. (2017). ATM, ATR, and DNA-PK: the trinity at the heart of the DNA damage response. *Mol. Cell* 66, 801–817.
71. Ceccaldi, R., Rondinelli, B., and D'Andrea, A.D. (2016). Repair pathway choices and consequences at the double-strand break. *Trends Cell Biol.* 26, 52–64.
72. Verma, R., Rigatti, M.J., Belinsky, G.S., Godman, C.A., and Giardina, C. (2010). DNA damage response to the Mdm2 inhibitor Nutlin-3. *Biochem. Pharmacol.* 79, 565–574.
73. Ran, F.A., Hsu, P.D., Wright, J., Agarwala, V., Scott, D.A., and Zhang, F. (2013). Genome engineering using the CRISPR-Cas9 system. *Nat. Protoc.* 8, 2281–2308.
74. Ling, X., Xie, B., Gao, X., Chang, L., Zheng, W., Chen, H., Huang, Y., Tan, L., Li, M., and Liu, T. (2020). Improving the efficiency of precise genome editing with site-specific Cas9-oligonucleotide conjugates. *Sci. Adv.* 6, eaaz0051.
75. Liu, Y., Yang, D., Wei, S., Nie, Y., Zhang, X., Lian, Z., and Han, H. (2018). Isolation and characterization of ovine monocyte-derived macrophages from peripheral blood. *Vet. Immunol. Immunopathol.* 205, 83–92.